Journal of Alloys and Compounds 501 (2010) 104–109

Contents lists available at ScienceDirect

Journal of Alloys and Compounds

journal homepage: www.elsevier.com/locate/jallcom

The study of the precipitation process in Al–Cu–Mg/bagasse ash particulate composites

V.S. Aigbodion*, S.B. Hassan

Department of Metallurgical and Materials Engineering, Ahmadu Bello University, Samaru, Zaria, Nigeria

ARTICLE INFO

Article history:
Received 2 December 2009
Received in revised form 1 April 2010
Accepted 10 April 2010
Available online 18 April 2010

Keywords:
Al–Cu–Mg alloy
Bagasse ash
Composites
Microstructure
Precipitation and thermal ageing

ABSTRACT

The phase formation and dissolution in Al–Cu–Mg/bagasse ash particulate composites have been studied by means of microstructural and differential scanning calorimetry (DSC) method. The composites were produced by double stir-casting method. 4 and 8 wt% bagasse ash particles were used in producing the composites. The DSC studies were carried out on the material in the as-quenched and the scanning electron microscopy analysis was carried out on the as-quenched and thermal aged specimens. In the aluminium alloy the effects of the reinforcement are similar to those observed by other authors with some remarkable features of the results. These include: a smaller amount of Guinier–Preston (GP) zones, faster precipitation kinetic of the intermediate phases (θ^{11} and θ^{1}) and absence of the peak related to the formation of the θ phase. The microstructure of the thermally aged composites at 200 °C for 6 h reveals the dissolution and distribution of the bagasse particle in the metal matrix and presence of precipitates at the particle matrix interfaces with precipitation and dissolution of the bagasse particles and (Al_2CuMg) phase.

1. Introduction

The accelerated ageing response observed in aluminium alloy composites has attracted considerable attention since the discontinuous ceramic reinforced composites were developed in the 1980s. It has been suggested in the literature that the enhanced precipitation kinetics in MMCs was caused by a higher dislocation density which is developed due to a large difference in the coefficients of thermal expansion (CTE) between the aluminium matrix and the ceramics [1].

Differential scanning calorimetry (DSC) is a common technique utilized in the investigation of the precipitate reactions in MMCs. Although the heating program used in the DSC scanning is different from that used in conventional isothermal ageing practice, it can provide a rapid and quantitative means of identifying the matrix precipitate characteristics [1,2]. Since the decomposition process of a solid solution is diffusion kinetics controlled process, the diffusion process during the isothermal ageing is the sole function of the ageing time, but it is a function of both the time and the temperatures in DSC temperature scanning. The precipitate reactions occur much quicker during DSC scanning, but the characteristics are unchanged [2,3], provided that a reasonable heating rate is used to overcome the inherent response time of the equipment [4]. In previous DSC studies, the most significant discovery was that the addition of ceramic reinforcement (SiC or Al_2O_3) to an aluminium alloy moved the exothermic reaction peaks, associated with the precipitation of metastable and stable phases, to lower temperatures, but did not alter the precipitation sequence in the matrix [2–4].

However, the results reported by Appendino et al. [5] and Bayourni et al. [6] in which a significant displacement of the reaction peaks to the lower temperature was observed, were obtained from SiC (both particulate and whisker) reinforced AA6O61 composites which contained 50% more Mg_2Si in the matrix than that in the parallel base alloy. It is possible that the faster precipitation kinetics observed in these experiments might in part arise from the difference in the Mg, Si content of the matrix alloy. Although no published study on the precipitation reaction of composites A2009/bagasse ash particle as reinforcement is yet available, hence the present work reports the results of a microstructure and DSC investigation on precipitation reaction of bagasse ash particulate reinforced A2009 composites which was intended to check previously published results and to clarify the different effects on the composites and the parallel base alloy. An identification of each exothermic reaction peak, with associated precipitates, in the DSC thermogram of A2009 was also attempted.

2. Materials and experimental procedure

The bagasse ash used in these study were characterized and the results shown in Table 1 [8]. Composites used in this study were A2009 Al–bagasse ash particles composites containing 4 and 8 wt% bagasse ash particles. The specimen was produced

* Corresponding author. Tel.: +234 8028433576.
E-mail addresses: aigbodionv@yahoo.com (V.S. Aigbodion), hassbolaji@yahoo.com (S.B. Hassan).

0925-8388/$ – see front matter © 2010 Elsevier B.V. All rights reserved.
doi:10.1016/j.jallcom.2010.04.052

Table 1
Composition and properties of bagasse ash particles.

Constituent formula	Cliftonite (C), quartz (SiO_2), moissanite (SiC), titanium oxide (Ti_6O) Ti_6O
Density	1.95 g/cm^3
Refractoriness	1600 °C
Color	Black

using the double stir-casting method [7,8] by keeping the percentage of copper and magnesium constant (3.7%Cu and 1.4%Mg) according to the recommended standard to produced alloy of type A2009 [8,9]. A control sample without the bagasse ash was also produced with this method. After casting, the specimen were homogenized at 550 ± 5 °C for 2 h, and then quenched into iced water [8]. The specimens were then cooled in liquid nitrogen until the DSC runs commenced. The specimens for microstructure study were later aged at 200 °C with ageing time of 6 h [8].

DSC was used to investigate reactivity in A2009 and its MMCs. A Seteram TG-DSC 11, manufactured in France, interfaced with a SETSOFT 2000 software was used in this work. All the specimen and crucibles used were weighed using an electronic balance (Schimadzu Corporation, Model AUW120D) [8]. The DSC was run in the vertical mode in order to create uniform heat distribution in the specimen and the reference. The specimen, which was 5 mm in diameter and 1 mm in thickness, weighed approximately 60 mg, and was placed in one of the pans; the other pan was pure aluminium used as a reference [4,8]. The output from the DSC was measured (in J/(kg °C)), and the net heat-flow to the reference relative to the sample was recorded as a function of the scanning temperature. The specimens were loaded in the DSC at room temperature, and each scan was conducted over a temperature range from 50 to 500 °C. A different heating rate of 5, 10, 15 and 20 °C/min were used in all scans. Dry nitrogen was introduced and passed through the calorimeter cell to minimize oxidation. The positions of the peak temperatures on the DSC thermograms were determined by direct measurement from the graph.

The microstructural analysis is carried out using scanning electron microscopy (SEM) model (JEOL-JSM 5600LV) on polished specimens taken from the centre of composites cylinder, the SEM was operated at an accelerating voltage of 5–20 kV.

The Kissinger-type expressions were used in calculating the activation energies from data obtained from non-isothermal experiments [10], since the experiment was non-isothermal heat treatment with a constant heating rate, θ (e.g., DSC experiments). Mittemeijer et al. [10] approximation, Eq. (1) showing an expression between the temperature for a fixed stage of transformation,T_f and the heating rate, θ, was used as shown below:

$$\ln\left(\frac{T_{y_f}^2}{\Phi}\right) = \frac{E}{RT_{y_f}} + \ln\beta_y \quad (1)$$

where β_{y_1} is the state variable fully determining that fixed state of transformation. The activation energy is determined from the slope of the straight line obtained by plotting $\ln(T_i^2/\Phi)$ vs. $(1/T_i)$.

3. Results

The various microstructures developed for both as-cast and thermally age-hardened samples are shown in Micrographs 1–6. The results of a DSC investigation undertaken to monitor the effect of bagasse ash particles on precipitation reactions in A2009 and its composites are presented in Figs. 1–3. While Figs. 4–6 show the plots used in calculating the activation energy. Tables 2 and 3 show the peaks temperatures and values of activation energy.

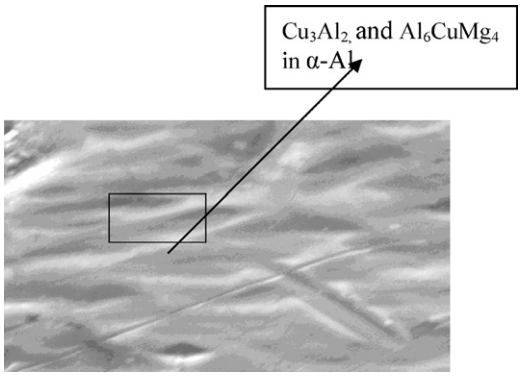

Micrograph 1. SEM microstructure of the unreinforced Al–Cu–Mg alloy (×100). The structure reveals the presence of Cu_3Al_2, Al_6CuMg_4 phases in α-Al matrix (white).

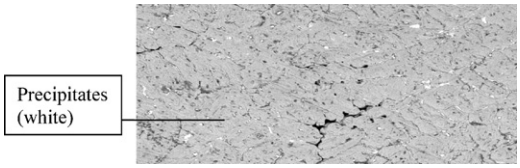

Micrograph 2. SEM microstructure of the Al–Cu–Mg alloy after thermally aged-hardened at 200 °C after peak aged (×100). The structure reveals dissolution and precipitation of Cu_3Al_2, and Al_6CuMg_4 (white) phases in α-Al matrix.

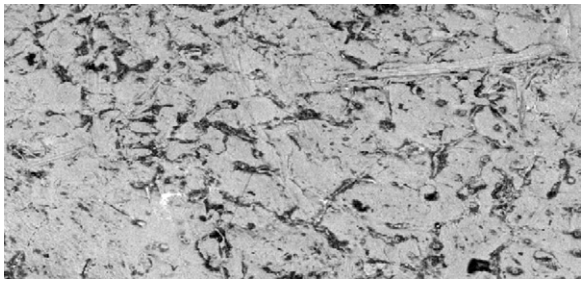

Micrograph 3. SEM microstructure of the reinforced Al–Cu–Mg alloy with 4 wt% bagasse ash/EDS spectrum (×100). The structure reveals the dissolution of the Cu_3Al_2, Al_6CuMg_4 phases and slight distribution of bagasse ash (black) in α-Al matrix (white).

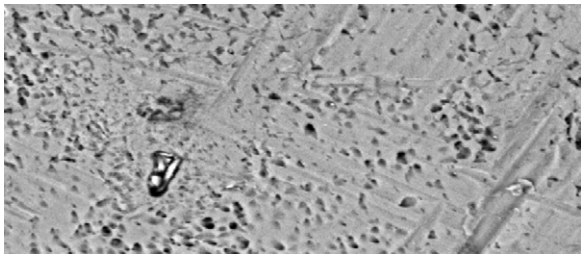

Micrograph 4. SEM microstructure of Al–Cu–Mg alloy reinforced alloy with 4 wt% of bagasse ash particle after thermally aged-hardened at 200 °C for after peak aged (×100). The structure reveals the dissolution of precipitation Cu_3Al_2, and Al_6CuMg_4 phase with good distribution of bagasse ash (black) in α-Al matrix with the formation of fine grains.

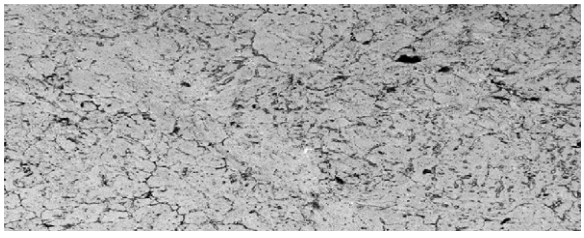

Micrograph 5. SEM microstructure of the reinforced Al–Cu–Mg alloy with 8 wt% bagasse ash (×100). The structure reveals the dissolution of the Cu_3Al_2, Al_6CuMg_4 phases and uniform distribution of bagasse ash (black) in α-Al matrix (white).

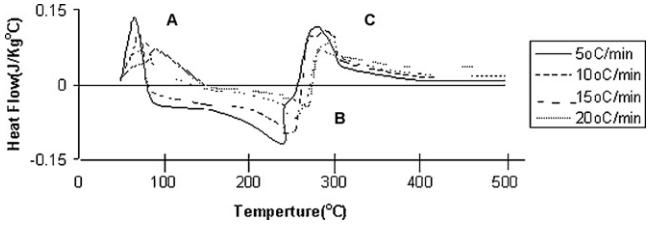

Fig. 1. The DSC scan of the unreinforced aluminium alloy at different heating rate.

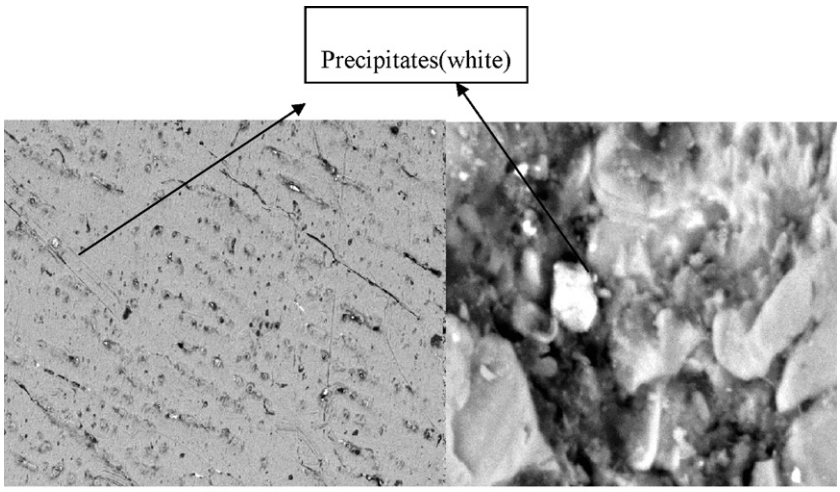

Micrograph 6. SEM microstructure of Al–Cu–Mg alloy reinforced alloy with 8 wt% of bagasse ash particle after thermally aged-hardened at 200 °C after peak aged. The structure reveals the dissolution and precipitation of the Cu_3Al_2, and Al_6CuMg_4 and uniform distribution of bagasse ash (black) in α-Al matrix, several sub-grain boundaries are visible.

4. Discussion

4.1. Microstructural study

The microstructure of the Al–Cu–Mg alloy reveals the eutectic phases containing Cu_3Al_2, and Al_6CuMg_4 in α-aluminium matrix (see Micrograph 1). In the as-cast condition, Cu and Mg are present both in solid solution with the matrix [4]. Jayalakshmi et al. [11] revealed that the general sequence of precipitation in Al–Cu–Mg alloys with Cu–Mg ratio of 2:1 is as follows [11]:

SS → GPB zones → S'' → S' → $S(Al_sCuMg)$

where GPB zones are Cu and Mg containing Guinier–Preston zones [11], and S' is a slightly strained semi coherent version of the incoherent S (Al_2CuMg) [11–12]. Since the formation enthalpies of the two variants are the same [4], S' and S will be considered to be the same phase in this study. The metastable S phase is the predominant precipitate in the Al–Cu–Mg alloy [4].

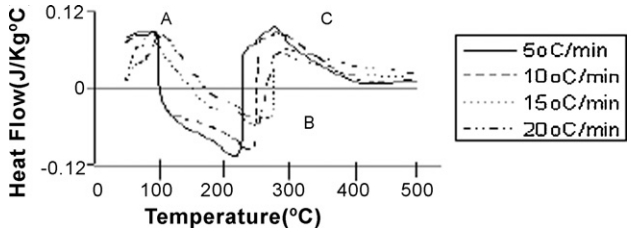

Fig. 2. The DSC scan of the reinforced aluminium alloy with 4% bagasse ash at different heating rate.

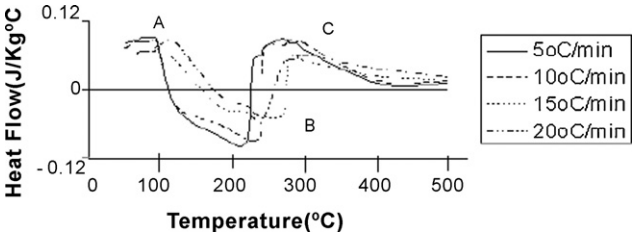

Fig. 3. The DSC scan of the reinforced aluminium alloy with 8% bagasse ash at different heating rate.

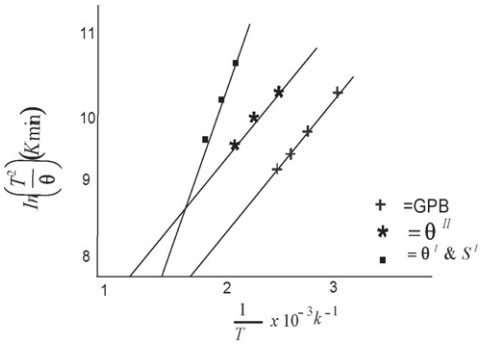

Fig. 4. Plot for the calculation of activation energy for the precipitate formation in unreinforced alloy (A2009).

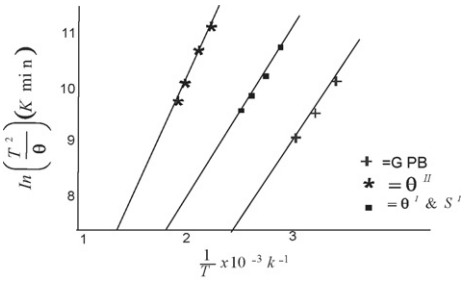

Fig. 5. Plot for the calculation of activation energy for the precipitate formation in reinforced alloy with 4 wt% bagasse ash.

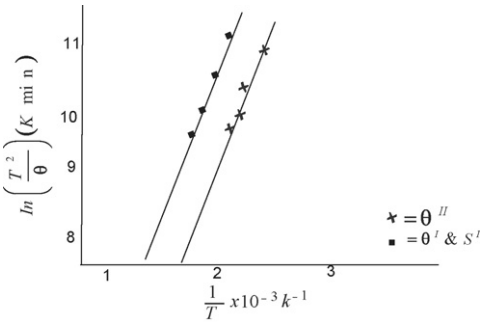

Fig. 6. Plot for the calculation of activation energy for the precipitate formation in reinforced alloy with 8 wt% bagasse ash.

Table 2
DSC peaks temperatures for unreinforced (A2009) and reinforced aluminium alloy with bagasse ash.

Heating rate (°C/min)	Peak A (°C) GPB zone	Peak B (°C) θ^{11}	Peak C (°C) S′ and θ′
DSC peak temperatures for 0 wt% bagasse ash addition			
5	64.00	240.00	280.00
10	72.50	240.70	291.00
15	81.00	255.50	300.08
20	92.90	270.00	310.00
DSC peak temperatures for 4 wt% bagasse ash addition			
5	–	225.00	276.00
10	92.90	230.80	280.00
15	95.60	250.00	295.00
20	107.00	257.70	300.50
DSC peak temperatures for 8 wt% bagasse ash addition			
5	–	220.00	271.00
10	–	228.00	278.00
15	–	240.00	289.40
20	120.00	245.00	297.50

A representative microstructure of the cast A2009 alloy reinforced with 4 and 8 wt% of bagasse ash particles are shown in Micrographs 3 and 5. The structure reveals a near-uniform distribution of the bagasse ash particles through the aluminium alloy metal matrix with no distinct evidence of clustering, or agglomeration is observed. This proves the effectiveness of the double stir-casting technique for producing composite microstructures.

Thermal ageing of the as-cast Al–Cu–Mg alloy enhances precipitation of the Cu_3Al_2, and Al_6CuMg_4 phases along grain boundaries (see Micrographs 2). The microstructure of the thermally aged composites reveal the dissolution and distribution of the bagasse particles in the metal matrix and presence of precipitates at the particles matrix interfaces with precipitation and dissolution of the bagasse particles and Cu_3Al_2, Al_6CuMg_4 phases (see Micrographs 4 and 6).

The formation and presence of precipitates at the particles–matrix interfaces may be appreciated by comparing micrographs of the composite in the as-cast state (Micrographs 3 and 5) and in the age-hardened state (Micrographs 4 and 6). The micrographs in the age-hardened state reveal precipitates covering the surface at the particles–matrix interfaces. This precipitation form may depends on Ref. [2]: (i) the extra interfacial area – and hence energy – between precipitate and matrix; (ii) the possible creation of an anti-phase boundary (APB) within an ordered precipitate and (iii) the change in separation distance between dissociated dislocations due to different stacking fault energies of matrix and particles. Similar behaviour of increased precipitation at interfaces was reported by Aigbodion and Hassan [7] for aluminum alloy reinforced with silicon carbide particle. They attributed this to increase in dislocation density at interfaces. Increase in dislocation density strain hardens the metal matrix locally and provides heterogeneous nucleation sites for precipitation, thereby accelerating the ageing response [3]. Thus, an increase in volume fraction of the reinforcing particles, fine grain size and distribution of these precipitates both within the grain and at grain boundaries contributes to acceleration of the aging kinetics.

Table 3
The activation energy (kJ/mol) of the precipitation process.

% of bagasse ash addition	GPB zone	θ^{11}	S′ and θ′
0	55.05	143.50	166.24
4	63.85	127.35	157.98
8	–	91.90	135.6

4.2. Differential scanning calorimeter (DSC) study

The curves in Figs. 1–3 consist of similar heat effects and the principal features of interest in this study are the two exothermic peaks, A and C, and the one endothermic effects B. Peak A is attributed to GPB zone formation [4] and it is a characteristic thermal effect in the *2xxx* series of aluminum alloys. Trough B has been ascribed to the dissolution of GPB zones (θ^{11})[4]. The second exothermic reaction zone C reveal single peak and has been ascribed (θ^{1})[3,4]. Peak C is not different from the single exothermic peak attributed by various workers [4] to precipitation of the S (Al_2CuMg) phase. Thus, the thermal effects associated with S′ → S transformation may not be sufficient to exhibit a separate peak during the DSC scan.

In rising-temperature techniques such as the DSC, the extent of transformation at any particular temperature can be controlled by thermodynamic equilibrium or kinetic limitations [1]. In thermally activated processes the heat effects shift to higher temperatures with increasing heating rate. Figs. 1–3 show that the formation and dissolution of GPB zones and the formation and dissolution of the S′ and θ′ phases are dominated by their reaction kinetics. The average values of the reaction peak temperatures associated with these transformations are shown in Table 2. The peak temperatures correspond to the points of maximum enthalpy of formation or dissolution [2]. The data in Figs. 1–3 as well as Table 2 show that the volume fraction of GPB phases formed in the unreinforced alloy is larger than that in the composite material. This has been reported by other workers [2,4] and has been explained in terms of the free vacancy concentration. Vacancies are required for the nucleation of GPB zones. The relatively high dislocation density found in the MMCs [4] on cooling from the fabrication solution heat treatment temperature gives rise to vacancy annihilation. Hence, with the vacancy concentrations being lower in the MMCs than the unreinforced alloys, fewer stable GPB zones are formed in the MMCs during DSC scans (see Figs. 2 and 3). However, this hypothesis cannot explain the observed higher GPB zone dissolution enthalpy usually obtained in the MMCs. Therefore, it is suggested that the smaller amount of GPB zones formed in the MMCs is due to a synergistic action of two competing phenomena, namely: (i) the prior precipitation of stable GPB zones during quenching and (ii) the decreased-vacancy-content phenomenon [4,12].

The peak temperature for GPB zone formation is less in the monolithic alloy than in the composite material. This suggests that GPB zone formation requires a lower driving force in the unreinforced alloy compared to the MMCs. Also the peak temperatures for GPB zone dissolution and θ′ + S′ formation are less in the composite compared to the unreinforced alloy.

The addition of bagasse ash particles affects not only the precipitation kinetics, but also the relative amounts of the various phases present. It reduced the amount of GPB zones formed in the MMCs relative to the unreinforced alloy. It is believed that this is due to the fact that some GPB zones have formed and stabilized prior to the DSC scan. That is, during quenching from the solution heat treatment temperature the bagasse ash particles cool more slowly than the matrix (since the particles have a lower thermal conductivity). This causes the matrix around the particles to be warmer than the bulk matrix. The high dislocation density and the high solubility centers (the warm particle–matrix interfaces) in the composite are favorable conditions for GPB zone formation. With a significant amount of GPB zones formed (in the composite) during quenching, the subsequent DSC scan yields a smaller amount of GPB zones in the composite than in the unreinforced alloy [2–4]. This mechanism is a possible explanation for the higher volume fraction of precipitates obtained in the composite during the endothermic GPB zone dissolution process than during the exothermic GPB zone formation.

The DSC peak A in both Figs. 1–3 due to GPB zone formation. These results imply by plotting $\ln(T_i^2/\Phi)$ vs. $(1/T_i)$ as shown in Figs. 4 and 5 the effective activation energies for GPB zone formation in both materials were obtained. These values agree fairly well with the results obtained from the AJM (Avrami–Johnson–Mehi) analysis [10].

The migration energy of vacancies in Al–Cu–Mg alloys has been reported to be in the range 41–66.9 kJ/mol [4]. The values of activation energy for GPB zone formation obtained in the present study for A2009 using the varying-heating rate method is 55.05 kJ/mol which are within this range, and are lower than those reported in the literature for Al–Cu–Mg alloys by Jena et al. [13] were $E = 55.6$ kJ/mol for Al–l.53 wt%Cu–0.79 wt%Mg alloy using the DSC technique. Papazian [14] reported $E = 61.0 \pm 2.2$ kJ/mol and $E = 53.9 \pm 1.6$ kJ/mol for A8090 using the DSC and resistivity techniques, respectively.

In MMCs, the ceramic particles have intermetallic particles which have different coefficient of thermal expansion from the Al-rich matrix. As such, on cooling from the solution heat treatment temperature they give rise to large amount of misfit dislocations. The dislocations and the large interfaces can act as vacancy sinks that annihilate excess vacancies needed for GPB zone nucleation [14].

The above calculations also show that GPB zone precipitation in the A2009 alloy reinforced with 4 wt% bagasse ash composite requires a higher driving force than in the unreinforced alloy. The suppression of GPB zone formation and its elevation to higher temperatures have been reported in some MMCs [4,14]. This has been attributed to the annihilation of quenched-in vacancies by misfit dislocations.

The amount of misfit dislocations generated in the composite material is larger than in the unreinforced alloy due to the large difference in the coefficients of thermal expansion (CTEs) of the matrix and the bagasse ash particles [2]. The presence of bagasse ash particles also creates large amounts of interfaces that can act as vacancy sinks. The low vacancy concentration in the composite matrix reduces the vacancy migration contribution to the GPB zone nucleation while increasing the contribution of substitution atom (Cu, Mg) migration. The latter process requires the creation of additional vacancies which consequently results in an increase in the calculated activation energy (E) of the reinforced alloy which is 63.85 kJ/mol.

The endothermic trough B in Figs. 1–3 is associated with GPB zone dissolution. Figs. 4–6 show, respectively, the variation of $\ln(T_i^2/\Phi)$ vs. $(1/T_i)$. Therefore, the GPB zone dissolution reaction is kinetically controlled in both unreinforced A2009 and the composite. The dissolution of GPB zones in some aluminum alloys has been attributed to a diffusion-limited mechanism [14]. The calculation of the kinetic parameters was carried out using Eq. (1) and the results are shown in Table 3. The value of activation energy obtained for A2009 using the Kissinger analysis ($E = 143.5$ kJ/mol) is greater than the value of 123.9 and 128.5 ± 3.5 kJ/mol reported in the literature [2,4], respectively. The concentration of quenched-in vacancies would be lower in A2009 than in the alloys studied by these workers [14].

The activation energy for solute diffusion during the GPB zone dissolution reaction includes the activation energy for formation of excess vacancies and that for solute transport. This implies lower effective activation energy for GPB zone dissolution in a vacancy-deficient environment than that in a vacancy-rich environment. The consequence is that the effective activation energy for GPB dissolution in the composite material was lower than that in the unreinforced alloy. However, in Table 2 the value of the effective activation energy obtained for the composite material ($E = 127.35$ and 91.9 kJ/mol) at 4 and 8 wt% bagasse ash addition are lower than that obtained for the unreinforced alloy ($E = 143.5$ kJ/mol).

Starink and Mourik [15] have reported that GPB zone dissolution reaction is essentially a two-step process. After the formation of GPB zone during a DSC scan, at least two reactions can occur on continued heating: (i) GPB zone dissolution (endothermic) and (ii) GPB zone coarsening (exothermic). In the present study, the temperature range of GPB zone dissolution during the DSC scan is conducive for solute diffusion. In the composite material, the local stress fields induced in the matrix by the presence of the reinforcements can give rise to enhanced matrix diffusivity (and hence accelerated dissolution kinetics) and a high dislocation density. Dislocations have been shown by both theoretical and experimental analyses [4,14,15] to serve as short-circuit paths for solute diffusion. Therefore, this could explain why GPB zone dissolution kinetics is enhanced in the composite material as compared to the unreinforced alloy.

The activation energy for S′ and θ′ formation A2009 alloy material from the slopes of the plots $\ln(T_i^2/\Phi)$ vs. $(1/T_i)$ in Figs. 4–6 is outside the range of values reported by previous workers. Jena et al. [13] obtained $E = 129.9$ kJ/mol for Al–3 wt%Cu–0.79 wt%Mg alloy, Youdelis and Fang [16] reported $E = 109.6 \pm 12.4$ kJ/mol, The discrepancy between the results obtained in the present work and the quoted data is attributed to differences in material composition, mass transfer resistance, and environment (matrix environment). Nevertheless, the values obtained for S′ and θ′ precipitation in this study are within the range of values reported in Ref. [15] ($E = 158$ kJ/mol) for A2214 aluminum alloy. The activation of energy of S′ and θ′ formation are lower in the MMCs than the unreinforced aluminium alloy, there are few published data in this area with which to compare the current results. Oscar [17], working on 2014 matrix composites, found the same trend as in the present work. Nieh and Karlak [18], working on 6xxx matrix MMCs, also found that the activation energy for diffusion was approximately 37% lower in the MMCs than in the unreinforced alloy. Nieh and Karlak [18] attributed the reduction in activation energy for diffusion in the MMCs to enhanced diffusion of solute along dislocations to growing transition precipitates. This could be the case in the current MMCs, with additional diffusion along the bagasse ash particles–matrix interfaces also contributing. As previously mentioned, the composite has a larger grain boundary area than the unreinforced alloy due to the smaller sub-grain size. This is likely to contribute to enhanced solute diffusion; Micrographs 4 and 6 can be used to support these facts.

5. Conclusions

From the analysis on the precipitation process on Al–Cu–Mg/bagasse ash composites, the following conclusions have been made:

1. The addition of bagasse ash particles to A2009 does not alter the aging sequence, but it alters certain aspects of the precipitation reaction. Although aging is accelerated in the composites and also the presence of bagasse ash particles in A2009 reduces the peak temperatures.
2. The kinetics of GPB zone formation in the MMCs is retarded when compared with those of the unreinforced alloy. On the other hand, the kinetics of GPB zone dissolution is more enhanced in the MMCs than in the unreinforced alloy.
3. The precipitation and dissolution of GPB zones and the metastable S′ and θ′ phases are kinetically controlled in both unreinforced A2009 and the composites. Hence, the addition of bagasse ash particles does not seem to alter the growth mechanisms for the formation of these metastable phases.
4. The kinetic parameters determined for the formation and dissolution of GPB zones using the Kissinger equation are, within

the limits of experimental errors, in good agreement with those other research obtained by the Kissinger-like expression.

5. Nucleation of precipitates in a cast A2009 matrix composite takes place on two different sites, namely: (1) quenched-in vacancy loops between the matrix and the reinforcement. Increasing reinforcement content increases nucleation on dislocations but, at the same time, it decreases vacancy concentration. Therefore, the contribution of quenched-in vacancies to the overall nucleation process is reduced.
6. A precipitation sequence for A2009/bagasse ash composites, based on the current DSC investigation, is proposed as: (i) formation and dissolution of GPB zones and (ii) concurrent formation and dissolution of metastable phases (S′ and θ′). That is:

$$\text{SSS} \rightarrow \text{GPB zones} \begin{cases} S' \rightarrow S \\ \theta' \rightarrow \theta \\ X' \rightarrow X \end{cases}.$$

References

[1] Y. Song, T.N. Baker, Mater. Sci. Eng. A 201 (1995) 251–260.
[2] M.J. Starink, P.J. Gregson, Scr. Metall. Mater. 33 (1995) 893–900.
[3] Y. Song, T.N. Baker, Mater. Sci. Technol. 10 (1994) 3739–3746.
[4] N.A.O. Ikechukwuka, Ph.D. Thesis, Department of Mechanical Engineering, University of Saskatchewan, Saskatoon, 1997, pp. 123–127.
[5] P. Appendino, C. Badini, F. Marino, A. Tomasi, Mater. Sci. Eng. A 135 (1991) 275–279.
[6] M. Bayourni, A.H. Ribes, M. Suéry, Aging characteristics of SiC-particle reinforced Al–Si alloys, in: Proc. 9th. Ris@ Inter. Symp. on Metallurgy and Materials Science, Ris@ National Laboratory, Roskilde, Denmark, 1988, pp. 291–296.
[7] V.S. Aigbodion, S.B. Hassan, J. Mater. Sci. Eng. A 447 (2007) 355–360.
[8] V.S. Aigbodion, Ph.D. work on-going, Department of Metallurgical and Materials Engineering, Ahmadu Bello University, Samaru, Zaria, Nigeria, 2008.
[9] Metals Handbook: Properties and Selection of Non-ferrous Alloys and Pure Metals, American Society of Metals (ASM), 1979, pp. 450–454.
[10] E.J. Mittemeijer, L. Cheng, P.J. van der Schaaf, C.M. Brakrnan, B.M. Kcxevaar, Metall. Trans. A 19A (1998) 925–932.
[11] S. Jayalakshmi, S. Seshan, S.V. Kailas, S. Srivatsan, Scr. Metall. Mater. (2004) 871–876.
[12] K.S. Ghosh, K. Das, U.K. Chatterjee, J. Mater. Sci. Technol. 20 (2004) 825–834.
[13] A.K. Jena, A.K. Gupta, M.C. Chaturvedi, Acta Metall. 37 (1989) 885–895.
[14] J.M. Papazian, Metall. Trans. A 13A (1982) 39.
[15] M.J. Starink, P. van Mourik, Mater. Sci. Eng. A 156 (1992) 183–194.
[16] W.V. Youdelis, W. Fang, Mater. Sci. Technol. 10 (1994) 1031–1041.
[17] M.S. Oscar, Mater. Charact. 49 (2003) 187–191.
[18] T.G. Nieh, R.F. Karlak, Scr. Metall. 18 (1984) 25–28.